ORIGINAL RESEARCH

Copper-Based Nanoparticles for Effective Treatment Against Sepsis-Induced Lung Injury in Mice Model

Jie-Mei Li[1,2,*], Lu Zhang[1,2,*], Sheng-Lin Pei[1,3], Liang Guo[1,3], Hong-Lei Shen [1,2], Jing He[1,2], You-Yuan Guo[1,2], Wei-Qing Zhang[4], Fei Lin [1,2]

[1]Department of Anesthesiology, Guangxi Medical University Cancer Hospital, Nanning, Guangxi, People's Republic of China; [2]Guangxi Health Commission Key Laboratory of Basic Science and Prevention of Perioperative Organ Disfunction, Nanning, Guangxi, People's Republic of China; [3]Guangxi Clinical Research Center for Anesthesiology, Nanning, Guangxi, People's Republic of China; [4]Department of Experimental Research, Guangxi Medical University Cancer Hospital, Nanning, Guangxi, People's Republic of China

*These authors contributed equally to this work

Correspondence: Fei Lin, Department of Anesthesiology, Guangxi Medical University Cancer Hospital, No. 71 hedi Road, Nanning, Guangxi, 530021, People's Republic of China, Tel +8613707886172, Fax +0086-771-536412, Email linfei@gxmu.edu.cn; Wei-Qing Zhang, Department of Experimental Research, Guangxi Medical University Cancer Hospital, No. 71 hedi Road, Nanning, Guangxi, 530021, People's Republic of China, Email zhangweiqing2008@hotmail.com

Introduction: Lung injury, a common complication of sepsis, arises from elevated reactive oxygen species (ROS), mitochondrial dysfunction, and cell death driven by inflammation. In this study, a novel class of ultrasmall nanoparticles ($Cu_{4.5}O$ USNPs) was developed to address sepsis-induced lung injury (SILI).

Methods: The synthesized nanoparticles were thoroughly characterized to assess their properties. In vitro experiments were conducted to determine the biologically effective concentration and elucidate the anti-inflammatory mechanism of action. These findings were further supported by in vivo studies, showcasing the material's efficacy in mitigating SILI.

Results: The $Cu_{4.5}O$ USNPs demonstrated remarkable scavenging capabilities for hydrogen peroxide (H_2O_2), superoxide anions (O_2^-), and hydroxyl radicals ($\cdot OH$), attributed to their catalase (CAT)- and superoxide dismutase (SOD)-like activities. Additionally, the nanoparticles exhibited strong anti-inflammatory effects, preserved mitochondrial homeostasis through potent ROS scavenging, and significantly reduced cell death. In vivo studies on mice further validated their protective role against SILI.

The conclusion: This study highlights the therapeutic potential of $Cu_{4.5}O$ USNPs in treating sepsis-induced lung injury by effectively scavenging ROS and reducing cell death. These findings provide compelling evidence for the future use of copper-based nanoparticles as antioxidant therapeutics.

Keywords: ultrasmall copper-based nanoparticles, mitochondria, reactive oxygen species scavenging, lung injury, anti-inflammation

Introduction

Severe sepsis can lead to multiorgan dysfunction, posing a life-threatening condition and imposing a significant global healthcare burden.[1–3] The lungs are particularly vulnerable in sepsis, significantly increasing mortality risk.[4–7] The pathogenesis of sepsis-induced lung injury (SILI) is closely tied to excessive production of reactive oxygen species (ROS), which upregulate proinflammatory cytokines and trigger an intense inflammatory response in pulmonary tissue.[8–11] Additionally, mitochondrial dysfunction, a key consequence of ROS overproduction, leads to reduced intracellular ATP levels, severely impairing cells' ability to maintain normal physiological activities.[12,13] Previous studies have shown that various forms of programmed cell death, often occurring simultaneously, are associated with mitochondrial dysfunction in conditions such as cerebral ischemia/reperfusion injury and glaucoma.[14–16] Therefore, finding effective strategies to protect mitochondria from ROS-induced damage is crucial.

Graphical Abstract
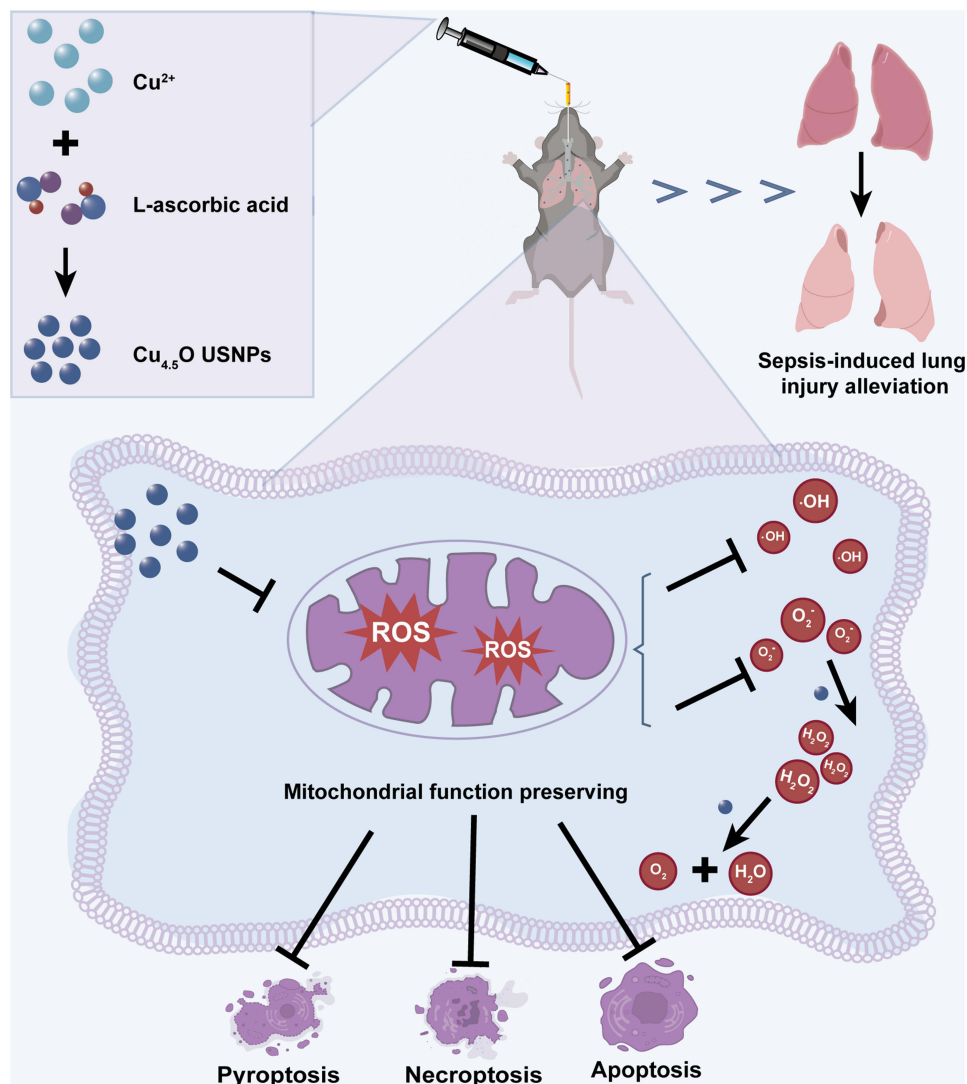
Nanomaterials offer distinct advantages, including biocompatibility, high targeting capabilities, and low toxicity,[17] making them innovative tools for scavenging ROS and addressing ROS-related diseases. Among them, mixtures of cuprous oxide (Cu_2O) and copper nanoparticles (Cu) have shown strong catalytic activity and ultrasmall dimensions, making them widely used as antioxidants.[18–21] Moreover, ultrasmall Cu-based nanoparticles can be synthesized in an eco-friendly manner, demonstrating superior long-term safety and stability compared to traditional bioenzymes,[22–24] making them promising candidates for therapeutic applications. To date, nanomaterials such as $Cu_{5.4}O$ USNPs[20] and $Cu_{4.6}O$ USNPs[21] have demonstrated ROS-inhibiting capabilities in models of glycerol-induced acute kidney injury and acute arterial embolism. However, their efficacy in treating acute systemic infections like sepsis, and the underlying biological mechanisms driving their effects, remain unclear.

In this study, based on the previously reported synthesis method of Cu and Cu_2O hybrid nanoparticles, we improved the proportion of Cu_2O in nanoparticles by making the reaction system in better contact with air to combat the complex oxidative microenvironment. We hypothesized that it could protect against acute inflammatory injuries caused by ROS in sepsis and preserve mitochondrial function. We evaluated its ROS-scavenging abilities both in vitro and in vivo, and

explored its potential to inhibit programmed cell death in lung tissue. Compared to Vitamin C, $Cu_{4.5}O$ USNPs-based therapy offers greater convenience and more efficacy. We hope this study inspires the application of artificial nanomaterials in developing therapies for sepsis.

Materials and Methods
Synthesis and Characterization of the Nanomaterial

$Cu_{4.5}O$ USNPs were synthesized using a green, environmentally friendly hydrothermal redox process.[20] All chemicals used were of at least analytical grade. Briefly, 50 mL of 10 mm anhydrous cupric chloride ($CuCl_2$, J&K Scientific, Beijing, China) was prepared under magnetic stirring in an open jar at 80 °C oil bath. Subsequently, 50 mL of freshly prepared 100 mm L-ascorbic acid (AA, J&K Scientific, Beijing, China) aqueous solution was slowly added while adjusting the pH to 8.0–9.0 using a 1 M NaOH solution (J&K Scientific, Beijing, China). The reaction mixture was maintained at 80 °C for 12 hours. Afterward, larger aggregates were removed by centrifugation at 7000 × g for 15 minutes. The supernatant was dialyzed against water (Mw: 10,000 Da) for two days to eliminate small molecules and ions, then lyophilized into a powder and stored at 4 °C.

The crystal structures of the $Cu_{4.5}O$ USNPs was confirmed using an X-ray diffractometer (XRD, Rigaku D/max 2500, Japan) with Cu Kα radiation (λ = 0.154598 nm).[25] The morphology of the nanoparticles was analyzed using field-emission transmission electron microscopy (TEM, Tecnai G2, Netherlands). X-ray photoelectron spectroscopy (XPS, ESCALAB 250Xi, Thermo Scientific, USA) was used to determine the surface chemical composition of the $Cu_{4.5}O$ USNPs.

Hydroxyl Radicals Scavenging Activity

The hydroxyl radical (·OH) scavenging activity of $Cu_{4.5}O$ USNPs was evaluated using an ·OH assay kit (Nanjing Jiancheng Bioengineering Institute, Nanjing, China).[20] The assay generates ·OH via the Fenton reaction. When electron acceptors interact with ·OH, a red-colored product forms with Griess reagent, displaying an absorption peak at 550 nm proportional to the amount of ·OH present. The addition of $Cu_{4.5}O$ reduced ·OH levels, as indicated by decreased absorption at 550 nm, measured using UV-vis spectroscopy (Spectrum, Shanghai, China).

Superoxide Anions Scavenging Activity

The scavenging activity of $Cu_{4.5}O$ USNPs against superoxide anions (O_2^-) was determined using an O_2^- assay kit (Nanjing Jiancheng Bioengineering Institute, Nanjing, China).[20] The absorbance of the Griess chromogenic agent at 550 nm gradually decreased with increasing concentrations of $Cu_{4.5}O$ USNPs, indicating reduced O_2^- levels. The scavenging ability at various concentrations was quantified based on the color intensity of the reaction system.

Hydrogen Peroxide Scavenging Activity

The hydrogen peroxide (H_2O_2) scavenging capacity of $Cu_{4.5}O$ USNPs was assessed using the 3,3′,5,5′-tetramethylbenzidine (TMB, Macklin, Shanghai, China) colorimetric method. In this reaction, we used our reported A-NiB@C-IrOx nanozymes]as peroxidase agents instead of horseradish peroxidase (HRP).[26] A 1 mL solution of 2 mm H_2O_2 (Nanjing Jiancheng Bioengineering Institute, China) was incubated with varying concentrations of $Cu_{4.5}O$ USNPs at 37 °C for 2 hours. Subsequently, a mixture of A-NiB@C-IrOx (1 μg/mL) and TMB (1 mm) was added. The reaction was incubated at 37 °C for 10 minutes, and the absorbance at 652 nm was recorded using UV-vis spectroscopy.

Radical Scavenging Assay

Radical scavenging activity was evaluated using previously reported methods.[20,27] Total antioxidant capacity (T-AOC) was measured using a 2,2′-azino-bis (3-ethylbenzothiazoline-6-sulfonic acid) diammonium salt (ABTS) assay kit (Nanjing Jiancheng Bioengineering Institute, Nanjing, China) following the manufacturer's instructions. First, the ABTS radical solution was prepared. The ABTS (7 mm) was dissolved in water, followed by the addition of 2.45 mm potassium persulfate. After incubation in the dark for 16 h, the resulting mixture was used to measure the absorbance of

ABTS at 734 nm. Second, the working solution (the ABTS radical solution mixed with the material at a ratio of 1:1) was prepared and allowed to react in the dark for 10 min. Finally, the working solutions at different concentrations of $Cu_{4.5}O$ USNPs were added to a multiple plate reader. The absorbance at 405 nm was measured after standing for 10 min via UV–vis spectroscopy.

The 1,1-diphenyl-2-picrylhydrazyl (DPPH) radical scavenging activity was assessed by dissolving (DPPH, Macklin, Shanghai, China) in anhydrous ethanol (500 μL, 100 μM) and mixing it with $Cu_{4.5}O$ USNPs in equal volumes.[28] The absorbance was measured at 517 nm.

Enzyme Activity

Catalase (CAT) is an enzyme that facilitates the decomposition of H_2O_2 into H_2O and O_2. Its activity can be determined by measuring the O_2 content.[29] We evaluated the CAT-like activity of $Cu_{4.5}O$ using two methods. In the first method, $Cu_{4.5}O$ USNPs were mixed with 10 mm H_2O_2, and the dissolved oxygen (DO) concentration was measured with a portable dissolved oxygen meter at room temperature. In the second method, various concentrations of $Cu_{4.5}O$ USNPs were incubated with 2 mM H_2O_2 at 37 °C for 2 hours. Titanium sulfate was then added to the reaction solution, which reacted with the remaining H_2O_2 to form a yellow peroxidation-titanium complex precipitate with a characteristic absorption peak at 415 nm.

The superoxide dismutase (SOD)-like activity of $Cu_{4.5}O$ USNPs was determined by assessing formazan formation using a SOD assay kit (WST-1 method; Nanjing Jiancheng Bioengineering Institute, Nanjing, China).[30] Briefly, O_2^- was generated by the oxidation of xanthine catalyzed by xanthine oxidase (XO), which converts WST-1 into WST-1 formazan, displaying a characteristic absorption at 450 nm. Formazan concentration was quantified at 450 nm using a multi-plate reader.

Animal Studies

C57BL/6J wild-type male mice (6–8 weeks old, weighing 20 ± 2 g) were obtained from the Animal Centre at Guangxi Medical University in Nanning, China. At the start of the experiment, the mice were randomly divided into three groups: control, LPS, and LPS + $Cu_{4.5}O$ USNPs group. Sepsis was induced by intraperitoneal injection of 20 mg/kg lipopoly-saccharide (LPS; Sigma, USA).[31] To determine the optimal concentration of $Cu_{4.5}O$ USNPs, the LPS + $Cu_{4.5}O$ USNPs group received intratracheal administration of $Cu_{4.5}O$ USNPs following LPS injection (n = 3). Subsequently, additional mice were divided into four groups: control, $Cu_{4.5}O$ USNPs, LPS, and LPS + $Cu_{4.5}O$ USNPs, and monitored twice daily for 10 days to assess survival rates (n = 10). Serum samples were collected 24 hours post-LPS injection or $Cu_{4.5}O$ USNPs treatment to evaluate ALT, AST, BUN, and CRE levels.

Enzyme-Linked Immunosorbent Assay and Hematoxylin & Eosin Staining

Proinflammatory mediators, including tumor necrosis factor-alpha (TNF-α) and interleukin-6 (IL-6), were quantified in lung tissue and serum samples using enzyme-linked immunosorbent assay (ELISA) kits (NeoBioscience Technology Co., Ltd., Shenzhen, China; n = 6). Lung tissues were fixed in 4% paraformaldehyde (Biosharp, Beijing, China) overnight and subsequently embedded in paraffin for sectioning. The sections were stained with a Hematoxylin and Eosin Staining Kit (Beyotime, Shanghai, China; n = 3), and images were captured using a light microscope (EVOS FL AutoLife Technologies, USA). The films were independently reviewed by two hospital pathologists using a double-blind methodology, and histopathological changes were assessed through random observation of three fields of view.

Western Blotting

Protein was extracted from lung tissue samples after treatment (n = 3). Equal amounts of protein were loaded onto a 12.5% SDS-polyacrylamide gel (YAMAY BIOTECH, Shanghai, China) for electrophoresis, followed by transfer to a polyvinylidene fluoride (PVDF) membrane (Bio-Rad, USA). The PVDF membrane was blocked with 5% milk for 1 hour and incubated overnight with primary antibodies against GSDMD-N (1:1000; ReXin Biotech, Quanzhou, China), P-MLKL (1:1000; ReXin Biotech, Quanzhou, China), and β-actin (1:10000; Affinity Biosciences, Australia).[32] The membrane was washed three times for 10 minutes each with TBST (Tris-buffered saline with Tween-20), then incubated

13510

International Journal of Nanomedicine 2024:19

with fluorescently labeled anti-rabbit secondary antibodies (1:10000; Abcam, UK) at room temperature in the dark for 1 hour. Following five washes of 5 minutes each, protein detection was performed using the Image Studio system, and quantitative analysis was conducted using ImageJ software.

TUNEL Staining

Paraffin-embedded tissue sections were deparaffinized in xylene and ethanol at room temperature, followed by incubation with proteinase K at 37 °C for 20 minutes to enhance tissue permeability. Next, equilibration buffer was added dropwise to cover the sample area entirely, and the sections were equilibrated for 10 minutes at room temperature. TdT incubation buffer was then applied, and the samples were incubated at 37 °C for 1 hour. Finally, DAPI staining was performed on the nuclei, and the sections were sealed with an anti-fluorescence quenching sealer. Fluorescence microscopy was used for observation.[33] All reagents were procured from Servicebio, Wuhan, China.

Hemolysis Rate

The hemolysis assay was adapted with minor modifications from previously established methods.[34] Fresh whole blood was obtained from the orbital veins of healthy C57BL/6J mice (n=3). After collection, the blood was centrifuged at 3000 rpm for 15 minutes to isolate red blood cells, which were then gently washed three times with PBS and diluted tenfold with PBS. $Cu_{4.5}O$ USNP concentrations of the various were adjusted to 5, 50, 500, and 5000 µg/mL using PBS as the diluent. A mixture of 0.2 mL of $Cu_{4.5}O$ USNP solution and 20 uL of red blood cell suspension was incubated for 3 hours at room temperature, followed by centrifugation. PBS and H_2O served as negative and positive controls, respectively. The supernatant (100 µL) from each mixture was transferred to a 96-well plate, and absorbance at 570 nm was measured spectrophotometrically to calculate the hemolysis rate.

Cell Culture and Cytotoxicity Assay

Mouse-derived mononuclear macrophages (RAW264.7 cells, obtained from Procell, Wuhan, China), pulmonary microvascular endothelial cells (MPVECs, Wuhan Fine Biotech Co., Ltd, China), lung epithelial cells (MLE12, BIOSPECIES, Guangzhou, China), and human myeloid leukemia mononuclear cells (THP-1, Procell, Wuhan, China) were utilized. RAW264.7 and MPVECs were cultured in Dulbecco's modified Eagle's medium (DMEM, Thermo Fisher Scientific, USA), THP-1 cells in Roswell Park Memorial Institute 1640 medium (RPMI, Servicebio, Wuhan, China), and MLE12 cells in endothelial cell medium (ScienCell, USA). All media were supplemented with 10% fetal bovine serum (FBS, Sigma-Aldrich) and 1% penicillin-streptomycin (Thermo Fisher Scientific, USA) and incubated at 37 °C under 5% CO_2.

RAW264.7, MPVECs, and MLE12 cells were seeded at 1×10^4 cells/well in 96-well plates, while THP-1 cells were seeded at 1×10^3 cells/well. After overnight incubation, cells were treated with varying concentrations of $Cu_{4.5}O$ USNPs for 24 hours. Subsequently, 10 µL of CCK-8 reagent (Vazyme Biotech Co., Ltd, Nanjing, China) was added to each well, followed by incubation at 37 °C for 1 hour. Absorbance at 450 nm was measured to assess cell viability.[35]

Calcein Acetoxymethyl Ester/Propidium Iodide Staining Assay and Apoptosis Flow Cytometry

RAW264.7 cells were seeded at 1×10^5 cells/well in 24-well plates and cultured overnight. The cells were then treated with LPS (1 µg/mL) or $Cu_{4.5}O$ USNPs for 24 hours.[36] Calcium green AM and propidium iodide (PI, Servicebio, Wuhan, China) were sequentially added, and the cells were incubated for 30 minutes. Fluorescence microscopy was used to capture images, assessing cell viability.[37]

For apoptosis analysis, RAW264.7 cells were seeded at 2×10^5 cells/well in 6-well plates and cultured overnight. After treatment with LPS or $Cu_{4.5}O$ USNPs for 24 hours, cells and supernatants were collected. Annexin V-APC (5 µL, BioLegend, USA) and 7-AAD (10 µL, BioLegend, USA) were added to the cell suspension and incubated in the dark at room temperature for 5 minutes. Apoptotic cells were analyzed using a CytoFLEX flow cytometer (Beckman Coulter, USA).

Intracellular Reactive Oxygen Species Scavenging Activity

RAW264.7 cells were seeded in 24-well plates at a density of 5×10^4 cells per well and cultured overnight. The cells were stimulated with LPS (1 μg/mL) for 24 hours, followed by treatment with $Cu_{4.5}O$ USNPs for an additional 24 hours. Next, the cells were incubated with 5 μM of the fluorescent probe 2.7-dichlorodihydrofluorescein diacetate (DCFH-DA) to detect ROS (Beyotime Biotechnology, Shanghai, China) and with O27 and O76 probes (Baiao Laibo, Beijing, China) diluted at 1:1000 to detect $\cdot OH$ and O_2^-, respectively. Incubation was carried out at 37 °C for 30 minutes.[38] Hoechst staining was used to label nuclei at 37 °C for an additional 15 minutes. The levels of intracellular ROS, $\cdot OH$, and O_2^- were observed using fluorescence microscopy. For quantitative ROS analysis, cells were seeded in 6-well plates under the same treatment conditions, then collected and analyzed via flow cytometry.

Measurement of Mitochondrial Superoxide

To measure mitochondrial superoxide levels, RAW264.7 cells were cultured overnight in 24-well plates at a density of 5×10^4 cells per well. After completing the specified treatments, cells were exposed to 1 μM MitoSOX reagent (Thermo Fisher, USA) and incubated at 37 °C for 30 minutes. Nuclei were subsequently stained with Hoechst.[39] Mitochondrial superoxide levels were visualized using a fluorescence microscope and quantified through flow cytometry.

Measurement of Mitochondrial Membrane Potential

RAW264.7 cells were treated as described previously. The JC-1 probe (Beijing Solarbio Science & Technology Co., Ltd., China) was diluted at a ratio of 1:100, and cells were incubated at 37 °C for 20 minutes.[40] Mitochondrial membrane potential (MMP) changes were visualized using fluorescence microscopy. In cells with high MMP, JC-1 forms aggregates within the mitochondrial matrix, emitting red fluorescence, whereas in cells with low MMP, the dye exists as monomers and emits green fluorescence.

ATP Assay

Following treatment, RAW264.7 cells were harvested, and intracellular ATP content was quantified using an ATP detection kit (Beyotime Biotechnology, Shanghai, China).[41] Cells were lysed using the provided lysis buffer, and 100 μL of ATP detection working solution was added to assay wells. After a 3–5 minute incubation at room temperature, 20 μL of either the sample or standard was added to the wells. Intracellular ATP levels were assessed by measuring relative light units (RLUs) using a luminometer.

Ultrastructure Under Transmission Electron Microscopy

The morphology and size of the $Cu_{4.5}O$ USNPs were characterized using a transmission electron microscope (TEM, H7560, Tokyo, Japan). For RAW264.7 cells, prefixation was performed by adding precooled 2.5% glutaraldehyde (Servicebio, Wuhan, China), followed by incubation for 1 hour. Cells were then collected, washed, and resuspended in 1 mL of fresh precooled 2.5% glutaraldehyde added carefully along the tube wall. After embedding in resin, ultrathin sections were prepared using an ultramicrotome and examined under TEM.[42]

Statistical Analysis

Experimental data were analyzed statistically using one-way analysis of variance (ANOVA) with GraphPad Prism 10 software. Quantitative results are presented as the mean ± standard error (SEM). The calculated probabilities (P) are represented as * $P < 0.05$, ** $0.001 < P < 0.01$, *** $0.0001 < P < 0.001$, **** $P < 0.0001$, and ns for not significant.

Results

In this study, we first synthesized the nanomaterials using previously established methods and analyzed their structural characteristics. The resulting nanomaterial exhibited a homogeneous, ultrafine nanoparticle structure with an average diameter of 2.8 nm (Figure 1A). As shown in Figure 1B, distinct peaks at $2\theta = 41.6°$, $50.7°$, and $77.5°$ correspond to the (111), (200), and (220) lattice planes of face-centered cubic copper, respectively.[20] Additionally, peaks at $2\theta = 29.6°$,
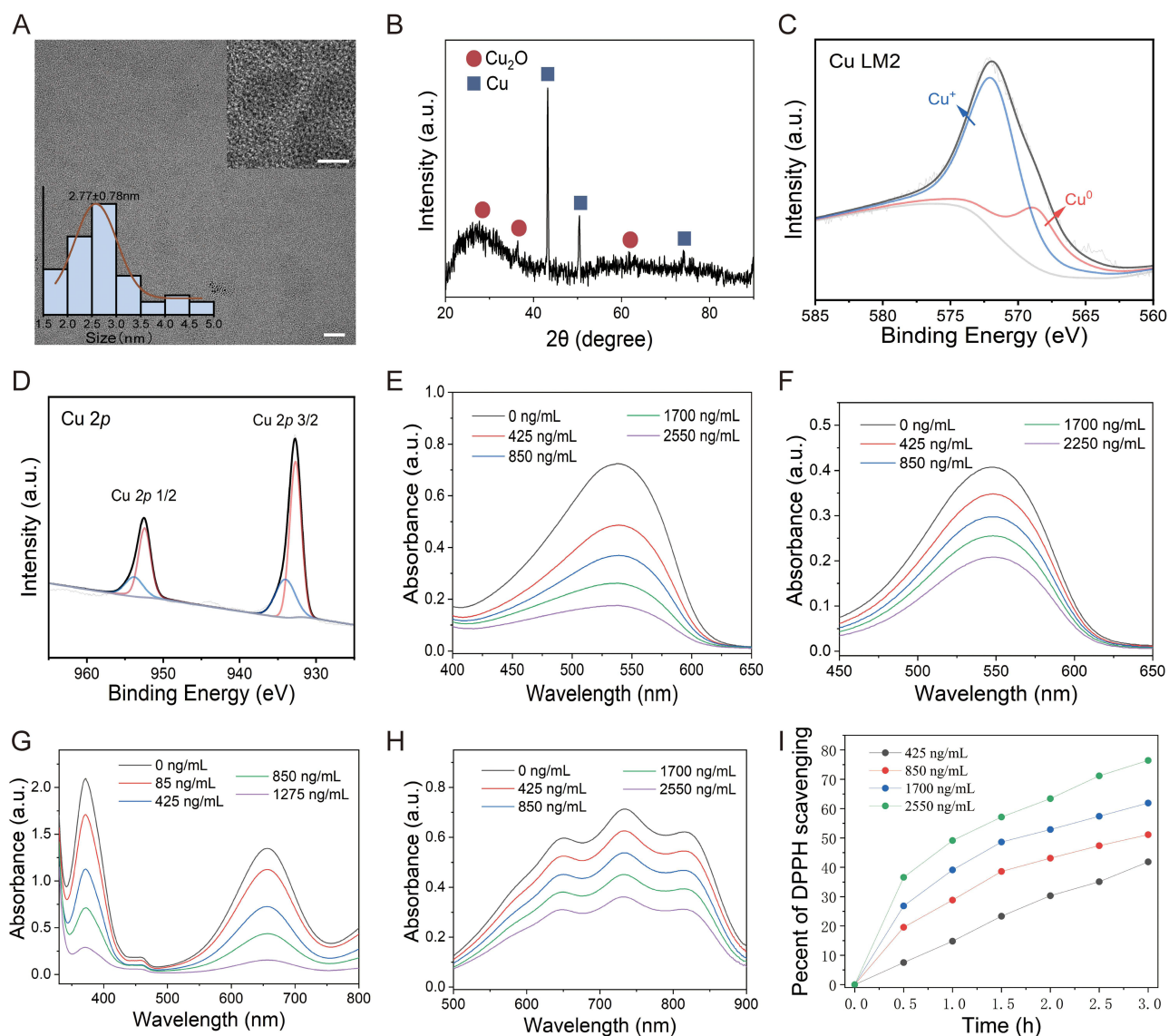
Figure 1 Structural characterization and ability of $Cu_{4.5}O$ USNPs. (**A**) Transmission electron microscopy images, with magnification scale bars of 100 nm and 5 nm. (**B**) Crystal structure under powder X-ray diffraction. Surface chemical composition under X-ray photoelectron spectroscopy in the Cu (**C**) LM2 spectrum and (**D**) $2p$ spectrum. (**E–I**) Reactive oxygen species scavenging activities of $Cu_{4.5}O$ USNPs: (**E**) ·OH, (**F**) O_2^-, (**G**) H_2O_2, (**H**) ABTS, and (**I**) DPPH.

36.4°, and 60.1° were attributed to the (110), (111), and (220) lattice planes of Cu_2O.[43–45] These results confirmed that the nanomaterial consisted of a mixture of Cu and Cu_2O nanoparticles. XPS survey spectra further validated the presence of Cu, C, and O in the nanoparticles (Figure S1). In the Cu LM2 spectrum, peaks at 571.8 and 568.6 eV were attributed to Cu+ and CuO, respectively (Figure 1C).[46,47] Similarly, the Cu $2p$ spectrum revealed peaks at 932.73 and 934.43 eV, corresponding to CuO and Cu+, respectively, based on the fitting results of Cu $2p$ 3/2 (Figure 1D).[20,48] Analysis of the Cu $2p$ peak areas indicated a Cu_2O to Cu ratio of 0.4:1 in the nanoparticles, leading to their designation as $Cu_{4.5}O$. Next, we conducted a series of experiments to verify the ROS scavenging activity and catalytic properties of $Cu_{4.5}O$ USNPs. The scavenging activity was evaluated for ·OH, O_2^- and H_2O_2. The results showed that scavenging efficiency increased with material concentration. A reduction in the absorption peak was observed as the concentration of ·OH decreased (Figure 1E). At a $Cu_{4.5}O$ USNP concentration of 2550 ng/mL, the O_2^- scavenging rate exceeded 50% (Figure 1F). Furthermore, H_2O_2 was nearly completely consumed at a concentration of 1275 ng/mL (Figure 1G). The absorbance of ABTS probes was negatively correlated with $Cu_{4.5}O$ USNP concentration (Figure 1H), consistent with findings from the T-AOC assay kit (ABTS method) (Figure S2A). After 3 hours of incubation with $Cu_{4.5}O$ USNPs, the DPPH probes were

effectively cleared, with the scavenging percentage increasing in a concentration-dependent manner ([Figures 1I](#) and [S2B](#)). The observed antioxidative properties of $Cu_{4.5}O$ USNPs were attributed to their enzyme-mimetic abilities. The CAT-like activity, which promotes the decomposition of H_2O_2 into H_2O and O_2, was evaluated using titanium sulfate. As $Cu_{4.5}O$ USNP concentrations increased, both CAT-like activity ([Figure S3A](#)) and DO levels significantly rose ([Figure S3B](#)). Additionally, $Cu_{4.5}O$ USNPs demonstrated significant concentration-dependent SOD activity ([Figure S3C](#)). These results confirmed the stable ROS and free radical scavenging capabilities of $Cu_{4.5}O$ USNPs, highlighting their potential as effective antioxidant enzymes.

After establishing the antioxidant properties of $Cu_{4.5}O$ USNPs, we investigated their intracellular performance. Cytotoxicity tests showed no significant changes in RAW264.7 cell viability, even at concentrations as high as 8500 ng/mL ([Figure 2A](#)), nor in
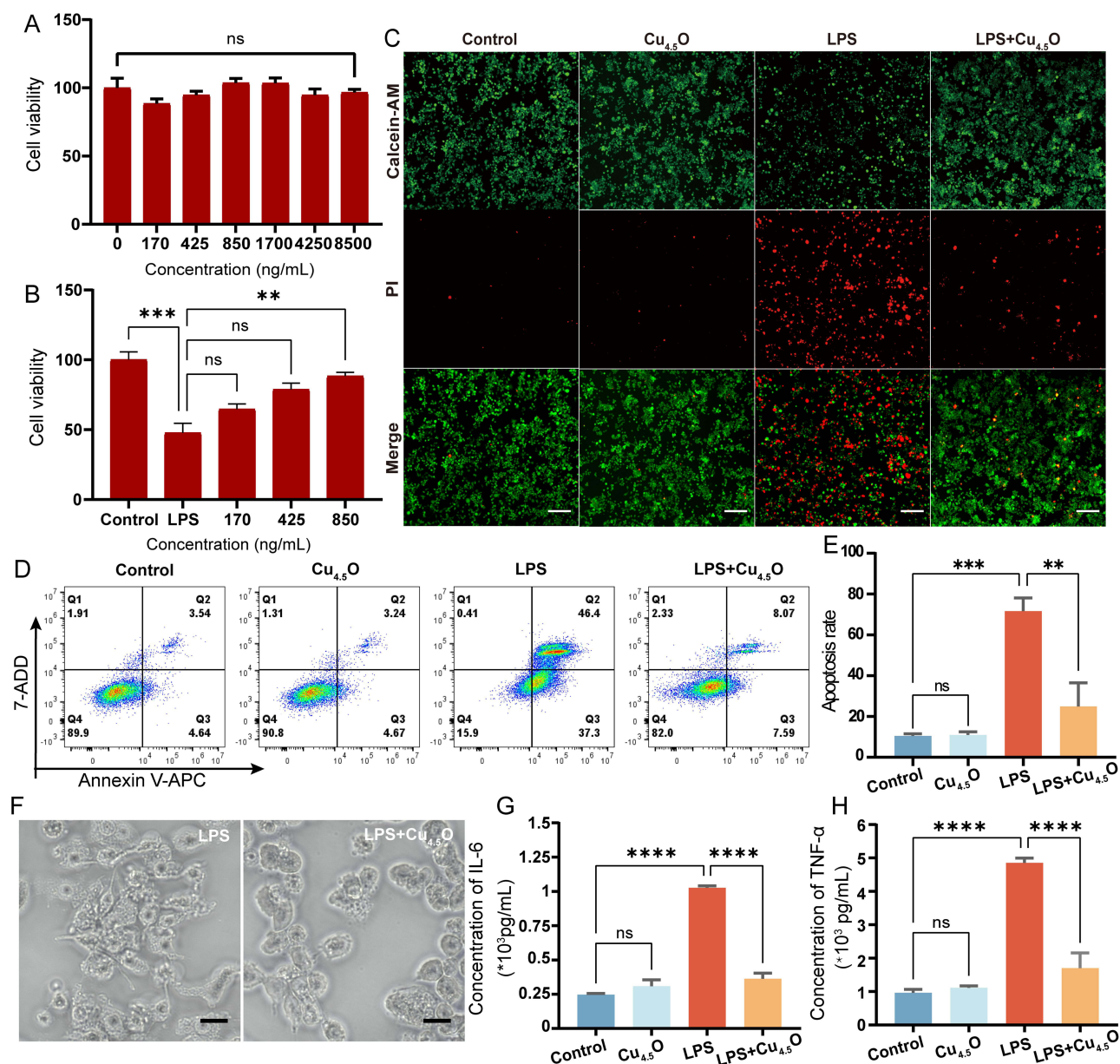

Figure 2 Cytotoxicity and therapeutic potential of $Cu_{4.5}O$ USNPs to the RAW 264.7 cell. (**A**) Cell viability of RAW264.7 cells cultured with various concentrations of $Cu_{4.5}O$ USNPs. (**B**) Therapeutic potential of $Cu_{4.5}O$ USNPs to LPS induced injury. (**C**) Calcein Acetoxymethyl Ester/Propidium Iodide staining of cells under an immunofluorescence microscope. The scale bar is 200 μm. (**D**) Flow cytometry results showing the percentage of apoptotic cells after different treatments and (**E**) Statistical analysis. (**F**) Bright-field image of RAW264.7 cells. The scale bar is 20 μm. (**G** and **H**) Inflammatory cytokine changes in cells treated with $Cu_{4.5}O$ USNPs at a concentration of 850 ng/mL. "**" = $0.001 < P < 0.01$, "***" = $0.0001 < P < 0.001$, "****" = $P < 0.0001$.
Abbreviations: LPS, Lipopolysaccharide; ns, no significant difference between groups.

THP-1, MPVECs, or MLE12 cells (Figure S4A–C). Subsequently, cells were exposed to LPS and varying concentrations of $Cu_{4.5}$ O USNPs. At a concentration of 850 ng/mL, the nanoparticles demonstrated notable therapeutic effects (Figures 2B and S5A–C). Macrophages, due to their pivotal roles in immune responses, are significant contributors to organ injury[49] and are prone to programmed cell death.[32,50] Therefore, intracellular experiments primarily focused on RAW264.7 cells. Fluorescence microscopy revealed bright green fluorescence in both the control and $Cu_{4.5}$O USNP-treated groups, indicating no cellular damage. Conversely, the LPS group displayed a higher proportion of dead cells, which was significantly reduced in the LPS + $Cu_{4.5}$ O USNP-treated group, showcasing the cytoprotective properties of the nanoparticles (Figure 2C). The percentage of apoptotic cells in the LPS + $Cu_{4.5}$O USNP group was 15.66%, significantly lower than the 83.70% observed in the LPS-only group ($p <$ 0.01; Figure 2D and E). RAW264.7 cells exposed to LPS for 24 hours exhibited morphological changes indicative of inflammation, including pseudopodia growth, fusiform shapes, and increased cell size. Treatment with $Cu_{4.5}$O USNPs effectively mitigated these changes (Figures 2F and S6), likely due to reduced inflammation in the LPS + $Cu_{4.5}$O USNP group (Figure 2G and H).

Notably, regulating the inflammatory cytokine response is critical in the pathophysiology of sepsis.[51,52] It has been reported that the overproduction of reactive oxygen species (ROS) contributes significantly to the progression of sepsis-induced inflammation.[53] In this study, we initially assessed intracellular ROS levels due to their strong correlation with sepsis. Using DCFH-DA staining, where green fluorescence indicates ROS presence, we observed that LPS stimulation induced excessive ROS generation. However, co-incubation with varying concentrations of $Cu_{4.5}$O USNPs significantly reduced ROS levels (Figure 3A).
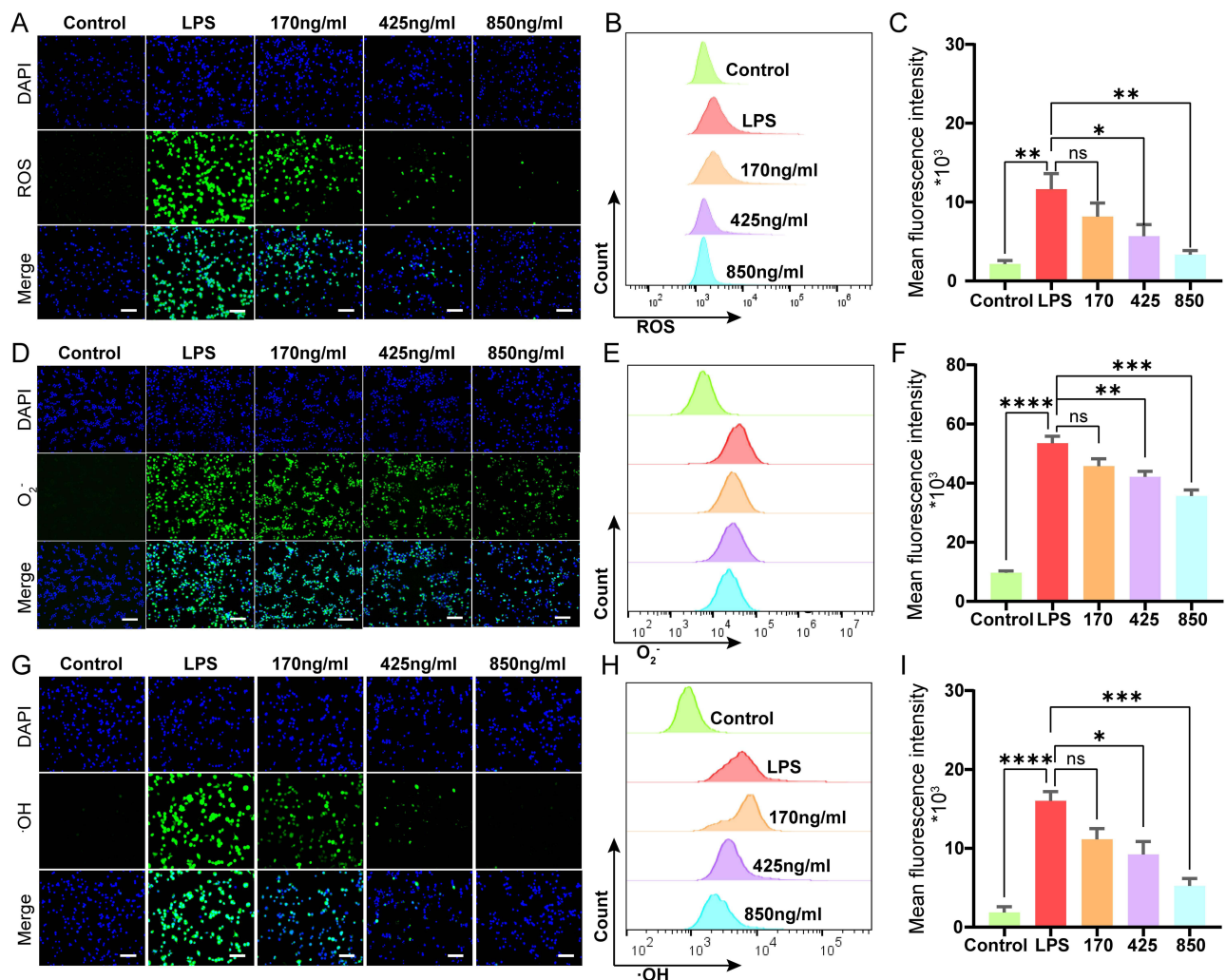

Figure 3 Combinations of fluorescence micrographs, flow cytometry intensity quantification and statistical analysis to demonstrate scavenging activity of $Cu_{4.5}$O USNPs in vitro. Scale bar is 100 μm in all fluorescence micrographs. (**A–C**) ROS. (**D–F**) O_2^-. (**G–I**) ·OH. "*" = $P < 0.05$, "**" = $0.001 < P < 0.01$, "***" = $0.0001 < P < 0.001$, "****" = $P < 0.0001$.
Abbreviations: ROS, Reactive Oxygen Species; LPS, lipopolysaccharide; ns, no significant difference between groups.

Flow cytometry further confirmed the stable ROS-scavenging activity of the nanoparticles (Figure 3B and C). Subsequent experiments focused on the scavenging capacity of ·OH and O_2^- using O27 and O76 probes. Both the fluorescence and flow cytometry results demonstrated significant scavenging activity against O_2^- (Figure 3D–F) and ·OH (Figure 3G–I). The results indicated that $Cu_{4.5}O$ USNPs had a concentration-dependent ability to scavenge ROS in cell.

Previous studies have shown that metal nanoparticles can protect cellular structures against inflammatory diseases.[54–57] Therefore, we further evaluated the protective effect of $Cu_{4.5}O$ USNPs on mitochondrial function by validating their ROS-scavenging activity and ability to restore ATP production. $Cu_{4.5}O$ USNPs preserved the normal structure of mitochondrial cristae (Figure 4A). Since mitochondrial membrane potential (MMP) decreases with mitochondrial damage, we assessed its status. LPS stimulation significantly reduced the MMP, whereas $Cu_{4.5}O$ USNPs effectively prevented this damage (Figures 4B and S7). Moreover, while LPS-induced mitochondrial instability caused a reduction in ATP production, treatment with $Cu_{4.5}O$ USNPs reversed this decline (Figure 4C). Fluorescence imaging further revealed that mitochondrial superoxide production induced by LPS was substantially suppressed by $Cu_{4.5}O$ USNPs (Figure 4D), a finding corroborated by flow cytometry (Figure 4E and F).

In animal studies, we evaluated the therapeutic potential of $Cu_{4.5}O$ USNPs in male C57BL/6J mice, as outlined in Figure 5A. Different concentrations of $Cu_{4.5}O$ USNPs were administered to septic mice, and treatment with 850 µg/kg $Cu_{4.5}O$ USNPs significantly mitigated lung damage (Figures 5B and S8). Hence, subsequent experiments utilized this concentration. Over ten days, no mortality was observed in the control or $Cu_{4.5}O$ USNPs groups. In contrast, the LPS group exhibited an 80% mortality rate. However, septic mice treated with $Cu_{4.5}O$ USNPs showed a significant improvement in survival, with a 60% increase compared to the LPS group, representing a twofold increase (Figure 5C). As shown in Figure 5D and E, the LPS group exhibited thickened alveolar walls, damaged alveolar structures, and significant inflammatory cell infiltration compared to the control and $Cu_{4.5}O$ groups. In contrast, septic mice treated with $Cu_{4.5}O$ USNPs showed reduced alveolar wall thickening and inflammatory cell infiltration, further demonstrating their protective effect against SILI. TNF-α and IL-6 were lower in lung tissue and serum samples from SILI mice treated with $Cu_{4.5}O$ USNPs (Figure 5F–I). $Cu_{4.5}O$ USNPs effectively counteracted the increase of superoxide levels caused by inflammation (Figure 6A). Apoptosis occurs as one phenomenon of programmed cell death.[58,59] The results exhibited a significant apoptosis of the LPS group, which was reversed by adding $Cu_{4.5}O$ USNPs (Figure 6B). Also, GSDMD-N and P-MLKL were significantly down-expressed provided the inhibited effect of $Cu_{4.5}O$ USNPs (Figure 6C–F).

There are different kinds of administration methods for nanoparticles.[60] Due to their unique properties, tracheal administration of $Cu_{4.5}O$ USNPs not only protected the lungs but also alleviated damage to other vulnerable organs from sepsis-induced injury. Histological analysis confirmed that the advanced administration of $Cu_{4.5}O$ USNPs ameliorated organ damage caused by sepsis (Figure 7A–H). Encouraged by these findings, we further examined liver and kidney function. Treatment with 850 µg/kg $Cu_{4.5}O$ USNPs significantly reduced key markers of organ dysfunction (Figure 7I–L). Intravenous administration was also assessed to evaluate safety and efficacy. $Cu_{4.5}O$ USNP injection did not cause significant organ damage and effectively mitigated multi-organ injury induced by LPS (Figure S9A–J). The hemolysis rate attributed to $Cu_{4.5}O$ USNPs was below 5%, demonstrating their biocompatibility (Figure S10). Lastly, we compared the therapeutic effects of $Cu_{4.5}O$ USNPs to Vitamin C for sepsis treatment. Results showed that a single intravenous dose of $Cu_{4.5}O$ USNPs (850 µg/kg) outperformed Vitamin C (50 mg/kg, administered every 6 hours) in preserving pathological features and reducing pulmonary edema (Figure S11).

Discussion

This study affirmed that $Cu_{4.5}O$ USNPs can effectively scavenge ROS, including ·OH, O_2^-, and H_2O_2, while also mimicking the activities of multiple enzymes such as CAT and SOD. Our findings demonstrate that $Cu_{4.5}O$ USNPs alleviate SILI in mice by preserving mitochondrial structure and function, maintaining mitochondrial membrane potential, and ensuring cellular energy supply. Furthermore, we revealed that $Cu_{4.5}O$ inhibit multi-programmed cell death pathways by downregulating key proteins. These results suggest that $Cu_{4.5}O$ USNPs hold significant promise as a therapeutic agent for treating sepsis-induced lung injury, highlighting their potential for combating acute systemic infections.
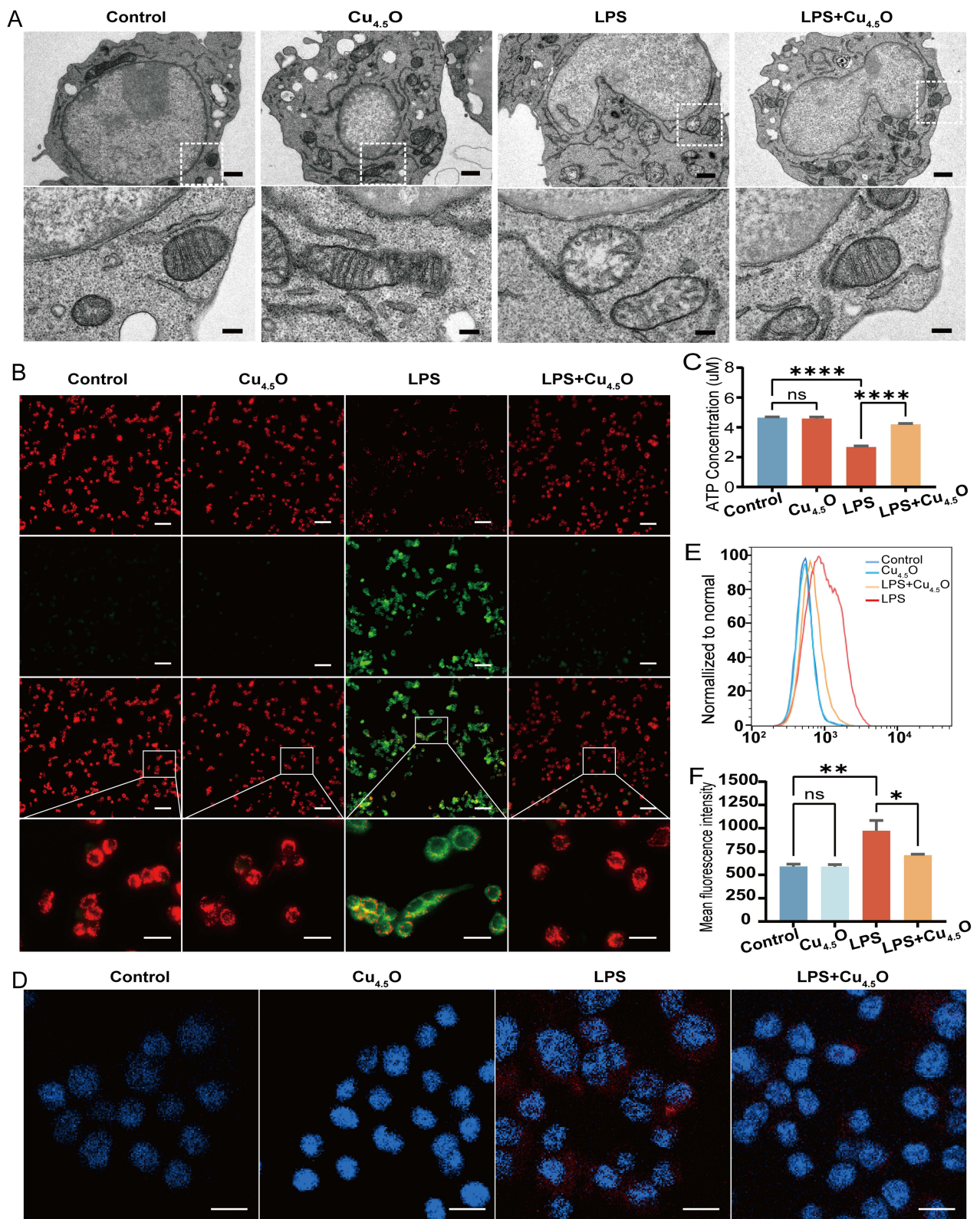
Figure 4 Cu$_{4.5}$O USNPs maintain mitochondrial stability in RAW 264.7 cell. (**A**) Structure of mitochondrial cristae under transmission electron microscopy. The scale bar is 1 μm in low field and 200 nm in high field. (**B**) Changes in mitochondrial membrane potential were visualized using a fluorescence microscope. The scale bar is 100 μm (low field) and 20 μm (high field). (**C**) Statistical analysis of ATP generation in each group. (**D**) Distribution of mitochondrial superoxides under a fluorescence microscope. The scale bar is 50 μm. (**E and F**) Detection and analysis of the mitochondrial superoxide levels by flow cytometry. "*" = $P < 0.05$, "**" = $0.001 < P < 0.01$, "****" = $P < 0.0001$.
Abbreviations: LPS, Lipopolysaccharide; ns, no significant difference between groups.
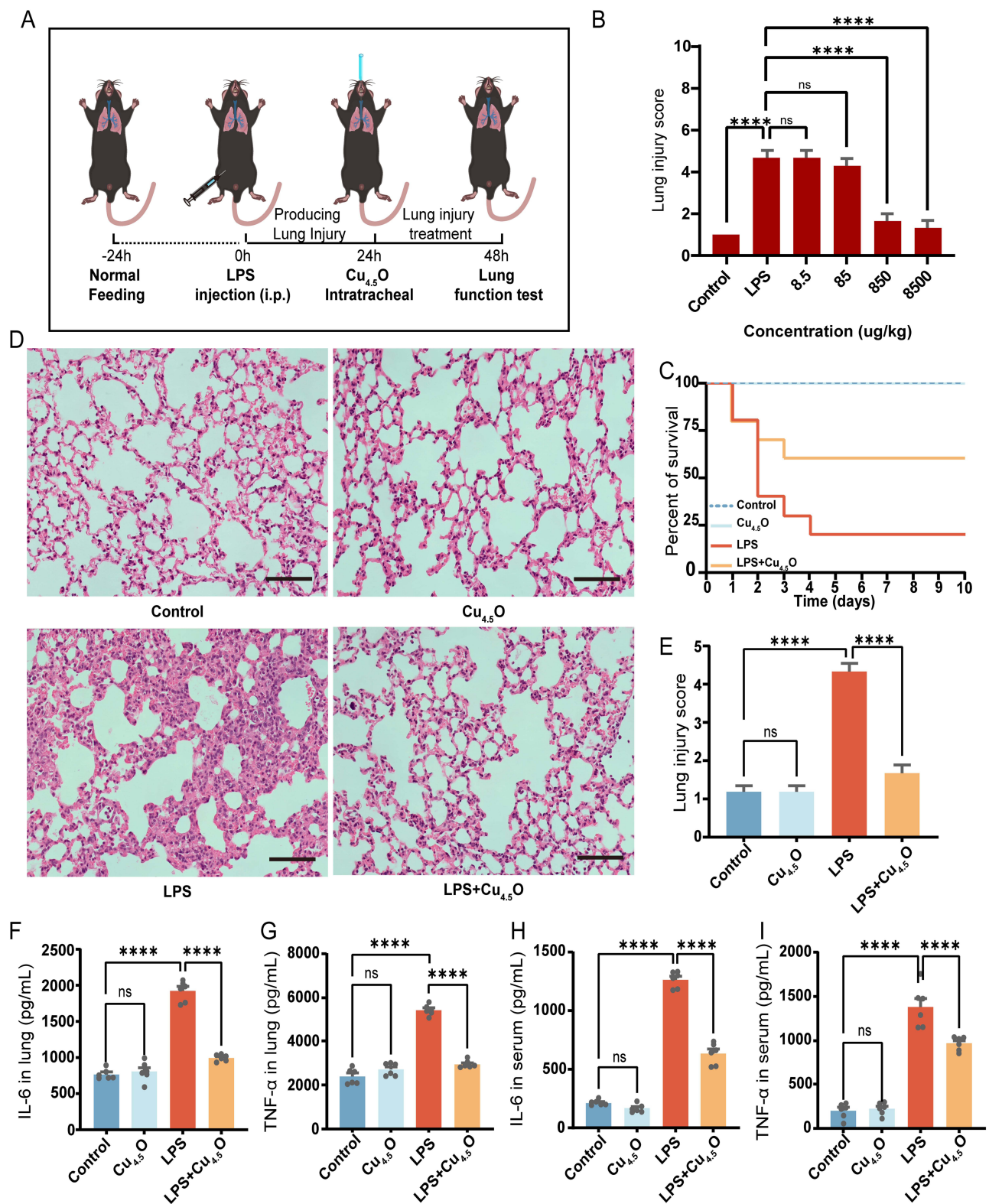
13517

Figure 5 Therapeutic efficacy of $Cu_{4.5}O$ USNPs in vivo. (**A**) Procedure for animal experiments. (**B**) Lung injury score in septic mice after receiving the concentration gradient of $Cu_{4.5}O$ USNPs, n=6. (**C**) Survival analysis, n=10. (**D**) Pathological structure and (**E**) injury degree of lung tissue was evaluated after with 850 μg/kg $Cu_{4.5}O$ USNPs. The scale bar is 50 μm. (**F** and **G**) Changes of IL-6 and TNF-α in Lung tissues and (**H** and **I**) serum, n=6. "****" = $P < 0.0001$.
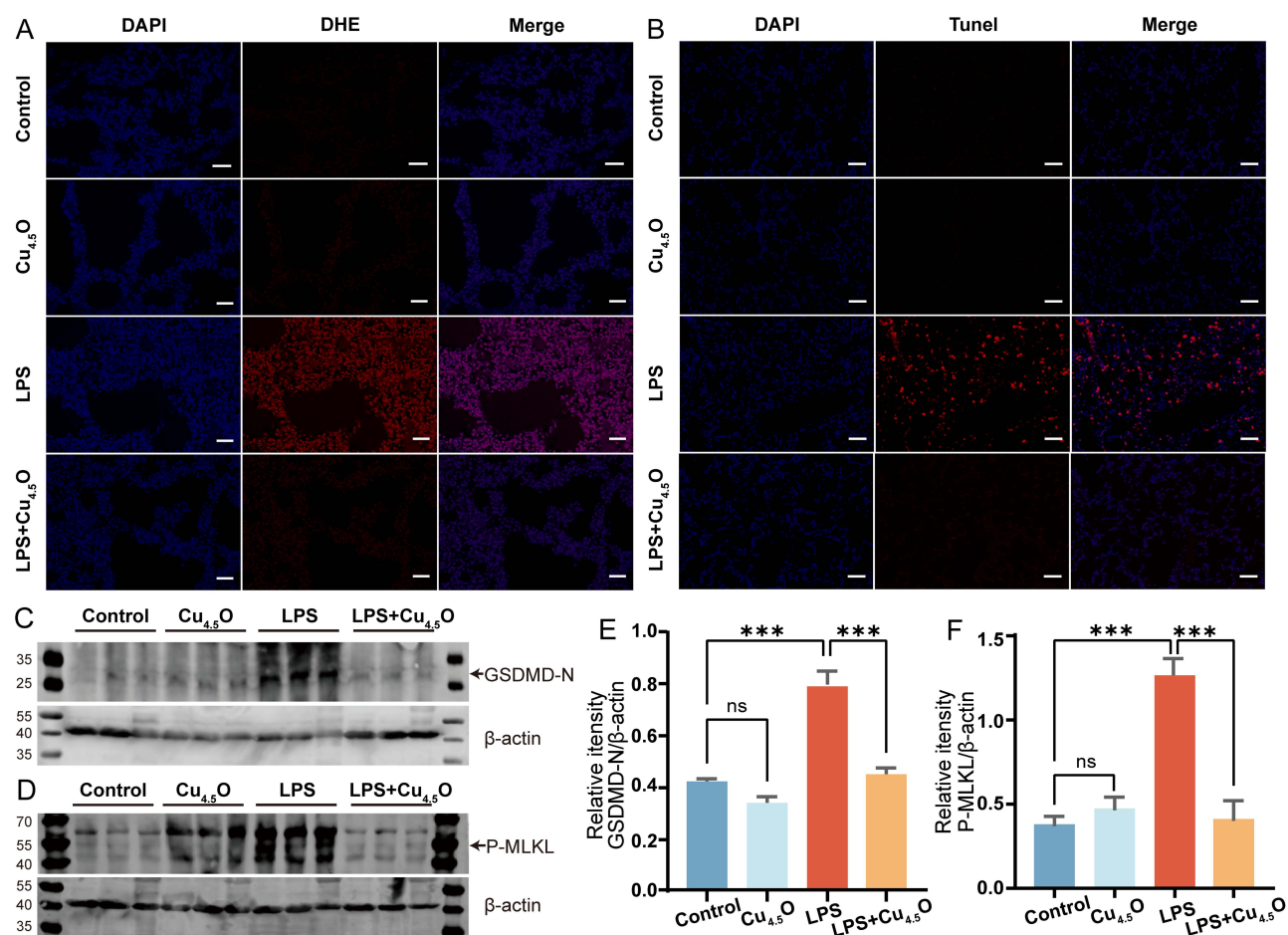**Abbreviations**: LPS, Lipopolysaccharide; ns, no significant difference between groups.

Figure 6 Cu$_{4.5}$O USNPs decrease lung oxidative damage in septic mice at a concentration of 850μg/kg. (**A**) Assessment of reactive oxygen species in the lungs of different groups by DHE staining. The scale bar is 50 μm. (**B**) Apoptosis of lung tissue, detected by the TUNEL method. The scale bar is 50 μm. The key protein of (**C**) pyroptosis and (**D**) necroptosis were detected by Western blotting which compare to β-actin expression (**E** and **F**). "***" = 0.0001 < *P* < 0.001. n=3.
Abbreviations: LPS, Lipopolysaccharide; ns, no significant difference between groups.

Cu$_{5.4}$O USNPs are the latest development in a series of copper-based ultrasmall nanoparticles known for their distinct aggregation profiles, stable properties, excellent biocompatibility, and water solubility. They effectively scavenge ROS, as demonstrated in prior studies on glycerinum-induced acute kidney injury.[20] These nanoparticles can absorb and neutralize free radicals due to their specialized surface, with copper ions further enhancing their antioxidant properties. Inspired by Liu et al[20] we synthesized Cu$_{4.5}$O USNPs following their methodology but achieved higher Cu$_2$O ratio, better coverage the scavenging spectrum of ·OH.

ROS are a class of highly reactive oxygen free radicals involved in a variety of cellular metabolic pathways, which can lead to oxidative stress and cause detrimental effects on cell structure and function.[61] It has been reported that the overproduction of ROS contributes to lung injury and facilitates its progression.[53] In the context of ROS generation, mitochondria undergo severe impairment, leading to diminished ATP synthesis, compromised mitochondrial membrane potential, and alterations in mitochondrial membrane permeability.[62] We verified that Cu$_{4.5}$O USNPs effectively preserved the structure and functionality of mitochondria, facilitating the maintenance of mitochondrial membrane potential and ensuring cellular energy supply. More importantly, we demonstrated the protective role of copper-based ultrasmall nanoparticles on subcellular organelles in LPS-induced sepsis, which is characterized by severe ROS stress.

PANoptosis is a coordinated cell death pathway.[58] Samir et al revealed that components of the PANoptosome, including Z-DNA-binding protein 1 (ZBP1), Gasdermin D (GSDMD), caspase-3, caspase-8, and the mixed lineage kinase domain-like pseudokinase (MLKL), are essential molecules for the activation of multi-programmed cell death.[59] In this study, we only tested the expression of key proteins in pyroptosis and necroptosis and observed apoptosis through
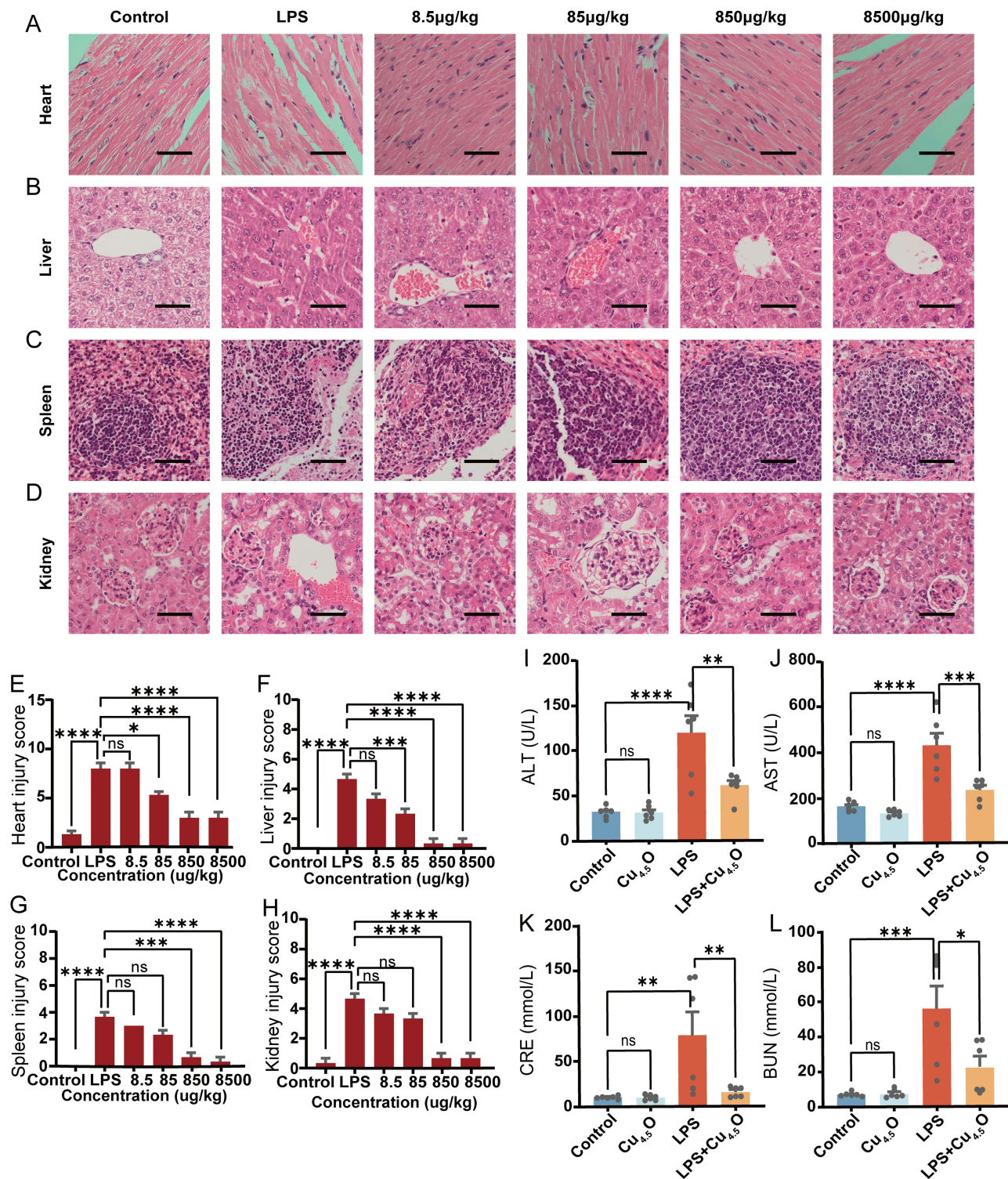
Figure 7 The therapeutic efficacy of Cu$_{4.5}$O USNPs in sepsis was assessed through histopathological analysis. (**A–D**) H&E staining of important organ tissues. All scale bars of H&E staining images are 50 μm, n=3. (**E–H**) Quantitative pathology scores in different organs, n=6. (**I–L**) Levels of organ function indicators in blood, n=6. "*" = $P < 0.05$, "**" = $0.001 < P < 0.01$, "***" = $0.0001 < P < 0.001$, "****" = $P < 0.0001$.
Abbreviations: LPS, Lipopolysaccharide; ALT, Alanine transaminase; AST, Aspartate aminotransferase; CRE, Creatinine; BUN, Blood Urea Nitrogen; ns, no significant difference between groups.

immunofluorescence. We discussed that $Cu_{4.5}O$ USNPs could attenuate pyroptosis and necroptosis, possibly because they effectively eliminate ROS, mitigate mitochondrial damage, and ultimately confer additional protection against programmed cell death.

In our study, tracheal administration was employed for the treatment of sepsis-induced lung injury. This approach reduces the total dose required and minimizes systemic exposure.[60,63] The results confirm that tracheal administration of $Cu_{4.5}O$ USNPs attenuates SILI, demonstrating significant potential for treating oxidative stress-related disorders. Currently, the primary treatments for sepsis involve anti-inflammatory drugs and antioxidants, such as Vitamin C.[64,65] However, these medications have limitations, including low bioavailability, poor stability, and limited efficacy in sepsis.[66] When using Vitamin C to alleviate lung injury, it is important to maintain therapeutic blood concentrations to sustain its antioxidative effects.[67] In contrast, our experimental results demonstrate that a single intravenous injection of $Cu_{4.5}O$ USNPs exhibits significantly stronger and more stable antioxidative capabilities within the effective range of Vitamin C. This highlights a key advantage of $Cu_{4.5}O$ USNPs for potential clinical applications.

This study has certain limitations. Our investigation primarily focused on mice, necessitating further studies to ensure the human safety of $Cu_{4.5}O$ USNPs. Additionally, it would be beneficial to design experiments comparing the efficacy of $Cu_{4.5}O$ USNPs with other nanomaterials previously reported for sepsis treatment. Finally, more detailed experiments are needed to elucidate how $Cu_{4.5}O$ attenuate PANoptosis. Nevertheless, our findings provide innovative insights for the research and development of optimized nanomedical materials targeting sepsis-induced lung injury.

Conclusion

This study validates that copper nanoparticles, $Cu_{4.5}O$ USNPs, possess remarkable ROS scavenging capabilities, which can be used to mitigate lung injury in sepsis. Importantly, we identified the pivotal role of $Cu_{4.5}O$ USNPs in maintaining mitochondrial homeostasis and inhibiting acute inflammation-induced cell death. Future research could explore biological distribution, metabolic dynamics, and comparisons with other nanomaterials or clinically effective drugs.

Data Sharing Statement

The data supporting this study's results are available from the corresponding author upon reasonable request.

Ethics Approval

All animal experiments were conducted following protocols approved by the Institutional Animal Care and Use Committee of Guangxi Medical University (Nanning, China, No. 202206009), in compliance with the Laboratory animals—General code of animal welfare (China, GB/T 42011-2022).

Acknowledgments

Acknowledgments to the reviewers and editors for their valuable insights.

Author Contributions

Wei-Qing Zhang and Fei Lin are Corresponding authors. All authors made a significant contribution to the work reported, whether that is in the conception, study design, execution, acquisition of data, analysis and interpretation, or in all these areas; took part in drafting, revising or critically reviewing the article; gave final approval of the version to be published; have agreed on the journal to which the article has been submitted; and agree to be accountable for all aspects of the work.

Funding

Disclosure

The authors report no conflicts of interest in this work.

References

1. Singer M, Deutschman CS, Seymour CW, et al. The third international consensus definitions for sepsis and septic shock (Sepsis-3). *JAMA*. 2016;315:801–810. doi:10.1001/jama.2016.0287
2. Oczkowski S, Alshamsi F, Belley-Cote E, et al. Surviving sepsis campaign guidelines 2021: highlights for the practicing clinician. *Pol Arch Intern Med*. 2022;132:16290. doi:10.20452/pamw.16290
3. Cecconi M, Evans L, Levy M, et al. Sepsis and septic shock. *Lancet*. 2018;392:75–87. doi:10.1016/S0140-6736(18)30696-2
4. Stapleton RD, Wang BM, Hudson LD, et al. Causes and timing of death in patients with ARDS. *Chest*. 2005;128:525–532. doi:10.1378/chest.128.2.525
5. Geyer-Roberts E, Lacatusu DA, Kester J, et al. Preventative management of sepsis-induced acute respiratory distress syndrome in the geriatric population. *Cureus*. 2023;15:e34680. doi:10.7759/cureus.34680
6. Xu C, Zheng L, Jiang Y, et al. A prediction model for predicting the risk of acute respiratory distress syndrome in sepsis patients: a retrospective cohort study. *BMC Pulm Med*. 2023;23:78. doi:10.1186/s12890-023-02365-z
7. Pravda J. Sepsis: evidence-based pathogenesis and treatment. *World J Crit Care Med*. 2021;10:66–80. doi:10.5492/wjccm.v10.i4.66
8. Zhang J, Zheng Y, Wang Y, et al. YAP1 alleviates sepsis-induced acute lung injury via inhibiting ferritinophagy-mediated ferroptosis. *Front Immunol*. 2022;13:884362. doi:10.3389/fimmu.2022.884362
9. Tsuji N, Tsuji T, Yamashita T, et al. BAM15 treats mouse sepsis and kidney injury, linking mortality, mitochondrial DNA, tubule damage, and neutrophils. *J Clin Invest*. 2023;133. doi:10.1172/jci152401
10. Lopes-Pires ME, Frade-Guanaes JO, Quinlan GJ. Clotting dysfunction in sepsis: a role for ROS and potential for therapeutic intervention. *Antioxidants*. 2021;11. doi:10.3390/antiox11010088
11. Chen Y, Ye Y, Krauß PL, et al. Age-related increase of mitochondrial content in human memory CD4+ T cells contributes to ROS-mediated increased expression of proinflammatory cytokines. *Front Immunol*. 2022;13:911050. doi:10.3389/fimmu.2022.911050
12. Mohsin M, Tabassum G, Ahmad S, et al. The role of mitophagy in pulmonary sepsis. *Mitochondrion*. 2021;59:63–75. doi:10.1016/j.mito.2021.04.009
13. van der Slikke EC, Star BS, van Meurs M, et al. Sepsis is associated with mitochondrial DNA damage and a reduced mitochondrial mass in the kidney of patients with sepsis-AKI. *Crit Care*. 2021;25:36. doi:10.1186/s13054-020-03424-1
14. Malireddi RKS, Kesavardhana S, Kanneganti TD. ZBP1 and TAK1: master regulators of NLRP3 inflammasome/pyroptosis, apoptosis, and necroptosis (PAN-optosis). *Front Cell Infect Microbiol*. 2019;9:406. doi:10.3389/fcimb.2019.00406
15. Zeng Z, You M, Fan C, et al. Pathologically high intraocular pressure induces mitochondrial dysfunction through Drp1 and leads to retinal ganglion cell PANoptosis in glaucoma. *Redox Biol*. 2023;62:102687. doi:10.1016/j.redox.2023.102687
16. She R, Liu D, Liao J, et al. Mitochondrial dysfunctions induce PANoptosis and ferroptosis in cerebral ischemia/reperfusion injury: from pathology to therapeutic potential. *Front Cell Neurosci*. 2023;17:1191629. doi:10.3389/fncel.2023.1191629
17. Ryabchikova E. Advances in nanomaterials in biomedicine. *Nanomaterials*. 2021;11:118. doi:10.3390/nano11010118
18. Zeng JY, Ding CP, Chen L, et al. Multienzyme-mimicking Au@Cu$_2$O with complete antioxidant capacity for reactive oxygen species scavenging. *ACS Appl Mater Interfaces*. 2023;15:378–390. doi:10.1021/acsami.2c16995
19. Fan WH, Wang XL, Cui MM, et al. Differential oxidative stress of octahedral and cubic Cu$_2$O micro/nanocrystals to Daphnia magna. *Environ Sci Technol*. 2012;46:10255–10262. doi:10.1021/es3011578
20. Liu T, Xiao B, Xiang F, et al. Ultrasmall copper-based nanoparticles for reactive oxygen species scavenging and alleviation of inflammation related diseases. *Nat Commun*. 2020;11:2788. doi:10.1038/s41467-020-16544-7
21. Kong JL, Zou R, Chu RX, et al. An ultrasmall Cu/Cu$_2$O nanoparticle-based diselenide-bridged nanoplatform mediating reactive oxygen species scavenging and neuronal membrane enhancement for targeted therapy of ischemic stroke. *Acs Nano*. 2023;18:4140–4158. doi:10.1021/acsnano.3c08734
22. Ke X, Xie BQ, Zhang JG, et al. Study on the preparation of ascorbic acid reduced ultrafine copper powders in the presence of different protectants and the properties of copper powders based on methionine protection. *Nanoscale Adv*. 2024;6:1135–1144. doi:10.1039/D3NA01146A
23. Menamo DS, Ayele DW, Ali MT. Green synthesis, characterization and antibacterial activity of copper nanoparticles using L-ascorbic acid as a reducing agent. *Ethiop J Sci Technol*. 2017;10(3):209–220. doi:10.4314/ejst.v10i3.5
24. Li MJ, Xiang K, Luo GQ, et al. Preparation of monodispersed copper nanoparticles by an environmentally friendly chemical reduction. *Chin J Chem*. 2013;31:1285–1289. doi:10.1002/cjoc.201300423
25. Kutukova K, Lechowski B, Grenzer J, et al. Laboratory high-contrast X-ray microscopy of copper nanostructures enabled by a liquid-metal-jet X-ray source. *Nanomaterials*. 2024;14(5):448. doi:10.3390/nano14050448
26. Wang Q, Shaik F, Lu XX, et al. Amorphous NiB@IrOx nanozymes trigger efficient apoptosis-ferroptosis hybrid therapy. *Acta Biomater*. 2023;155:575–587. doi:10.1016/j.actbio.2022.10.048
27. Wang B, Wang YM, Chi CF, et al. Isolation and characterization of collagen and antioxidant collagen peptides from scales of croceine croaker (Pseudosciaena crocea). *Mar Drugs*. 2013;11:4641–4661. doi:10.3390/md11114641
28. Tian Q, Wang W, Cao L, et al. Multifaceted catalytic ROS-scavenging via electronic modulated metal oxides for regulating stem cell fate. *Adv Mater*. 2022;34:e2207275. doi:10.1002/adma.202207275
29. Baker A, Lin CC, Lett C, et al. Catalase: a critical node in the regulation of cell fate. *Free Radic Biol Med*. 2023;199:56–66. doi:10.1016/j.freeradbiomed.2023.02.009
30. Zhang L, Jin W, Hu M, et al. Silencing miR-155-5p expression improves intestinal damage through inhibiting inflammation and ferroptosis in necrotizing enterocolitis. *Heliyon*. 2024;10(17):e37087. doi:10.1016/j.heliyon.2024.e37087
31. Asari Y, Majima M, Sugimoto K, et al. Release site of TNF alpha after intravenous and intraperitoneal injection of LPS from Escherichia coli in rats. *Shock*. 1996;5:208–212. doi:10.1097/00024382-199603000-00007

32. Zhang HR, Li YP, Shi ZJ, et al. Triptolide induces PANoptosis in macrophages and causes organ injury in mice. *Apoptosis*. 2023;28(11–12):1646–-1665. doi:10.1007/s10495-023-01886-6

33. Xue C, Sowden M, Berk BC. Extracellular cyclophilin A, especially acetylated, causes pulmonary hypertension by stimulating endothelial apoptosis, redox stress, and inflammation. *Arteriosclerosis Thrombosis Vasc Biol*. 2017;37(6):1138–1146. doi:10.1161/ATVBAHA.117.309212

34. Duan L, Zuo J, Zhang F, et al. Magnetic targeting of HU-MSCs in the treatment of glucocorticoid-associated osteonecrosis of the femoral head through Akt/Bcl2/Bad/Caspase-3 pathway. *Int J Nanomed*. 2020;15:3605–3620. doi:10.2147/IJN.S244453

35. Yang H, Ping X, Cui Y, et al. Role of Rapamycin and 3-MA in oxidative damage of HLECs caused by two doses of UVB radiation. *Adv Ophthalmol Pract Res*. 2023;3(1):15–22. doi:10.1016/j.aopr.2022.09.002

36. Zou P, Yang F, Ding Y, et al. Lipopolysaccharide downregulates the expression of ZO-1 protein through the Akt pathway. *BMC Infect Dis*. 2022;22(1):774. doi:10.1186/s12879-022-07752-1

37. Fan Y, Zhang W, Iqbal Z, et al. Rod-shaped mesoporous silica nanoparticles reduce bufalin cardiotoxicity and inhibit colon cancer by blocking lipophagy. *Lipids Health Dis*. 2024;23(1):318. doi:10.1186/s12944-024-02301-y

38. Haileselassie B, Joshi AU, Minhas PS, et al. Mitochondrial dysfunction mediated through dynamin-related protein 1 (Drp1) propagates impairment in blood brain barrier in septic encephalopathy. *J Neuroinflammation*. 2020;17(1):36. doi:10.1186/s12974-019-1689-8

39. Zhang T, Feng L, Cui J, et al. Hexavalent chromium induces neurotoxicity by triggering mitochondrial dysfunction and ROS-mediated signals. *Neurochem Res*. 2024;49(3):660–669. doi:10.1007/s11064-023-04063-y

40. Feng F, Ren Q, Wu S, et al. Hoxa5 increases mitochondrial apoptosis by inhibiting Akt/mTORC1/S6K1 pathway in mice white adipocytes. *Oncotarget*. 2017;8(56):95332–95345. doi:10.18632/oncotarget.20521

41. Shen Q, Yuan Y, Li Z, et al. Berberine ameliorates septic cardiomyopathy through protecting mitochondria and upregulating Notch1 signaling in cardiomyocytes. *Front Pharmacol*. 2024;15(1502354). doi:10.3389/fphar.2024.1502354

42. Wang Z, Chen M, Pan X, et al. Knockout of GGPPS1 restrains rab37-mediated autophagy in response to ventilator-induced lung injury. *Human Cell*. 2022;35(3):871–884. doi:10.1007/s13577-022-00692-7

43. Cheng Y, Bo H, Qin R, et al. Hyaluronic acid-coated Bi: cu$_2$O: an H$_2$S-responsive agent for colon cancer with targeted delivery and enhanced photothermal performance. *J Nanobiotechnology*. 2022;20:346. doi:10.1186/s12951-022-01555-x

44. Hu Q, Wang F, Fang Z, et al. Cu$_2$O-Au nanocomposites for enzyme-free glucose sensing with enhanced performances. *Colloids Surf B Biointerfaces*. 2012;95:279–283. doi:10.1016/j.colsurfb.2012.02.023

45. Yang N, Guo H, Cao C, et al. Infection microenvironment-activated nanoparticles for NIR-II photoacoustic imaging-guided photothermal/chemodynamic synergistic anti-infective therapy. *Biomaterials*. 2021;275:120918. doi:10.1016/j.biomaterials.2021.120918

46. Chen GF, Yuan YF, Jiang HF, et al. Electrochemical reduction of nitrate to ammonia via direct eight-electron transfer using a copper-molecular solid catalyst. *Nat Energy*. 2020;5:605–613. doi:10.1038/s41560-020-0654-1

47. Kim JY, Hong D, Lee JC, et al. Quasi-graphitic carbon shell-induced Cu confinement promotes electrocatalytic CO$_2$ reduction toward C$_{2+}$ products. *Nat Commun*. 2021;12. doi:10.1038/s41467-021-24105-9

48. Wang XR, Hung TF, Chen FR, et al. In situ tracking of crystal-surface-dependent Cu$_2$O nanoparticle dissolution in an aqueous environment. *Environ Sci Technol*. 2023;57(2):1006–1016. doi:10.1021/acs.est.2c07845

49. Jiao Y, Zhang T, Zhang C, et al. Exosomal miR-30d-5p of neutrophils induces M1 macrophage polarization and primes macrophage pyroptosis in sepsis-related acute lung injury. *Crit Care*. 2021;25:356. doi:10.1186/s13054-021-03775-3

50. Choudhury SM, Sarkar R, Karki R, et al. A comparative study of apoptosis, pyroptosis, necroptosis, and PANoptosis components in mouse and human cells. *PLoS One*. 2024;19:e0299577. doi:10.1371/journal.pone.0299577

51. Deng P, Tang N, Li L, et al. Diagnostic value of combined detection of IL-1β, IL-6, and TNF-α for sepsis-induced cardiomyopathy. *Med Clin*. 2022;158:413–417. doi:10.1016/j.medcli.2021.04.025

52. Faix JD. Biomarkers of sepsis. *Crit Rev Clin Lab Sci*. 2013;50:23–36. doi:10.3109/10408363.2013.764490

53. Liu C, Zou Q, Tang H, et al. Melanin nanoparticles alleviate sepsis-induced myocardial injury by suppressing ferroptosis and inflammation. *Bioact Mater*. 2023;24:313–321. doi:10.1016/j.bioactmat.2022.12.026

54. Alyami NM, Almeer R, Alyami HM. Role of green synthesized platinum nanoparticles in cytotoxicity, oxidative stress, and apoptosis of human colon cancer cells (HCT-116). *Heliyon*. 2022;8:e11917. doi:10.1016/j.heliyon.2022.e11917

55. Ye M, Zhao Y, Wang Y, et al. NAD(H)-loaded nanoparticles for efficient sepsis therapy via modulating immune and vascular homeostasis. *Nat Nanotechnol*. 2022;17:880–890. doi:10.1038/s41565-022-01137-w

56. Li C, Zhao Z, Luo Y, et al. Macrophage-disguised manganese dioxide nanoparticles for neuroprotection by reducing oxidative stress and modulating inflammatory microenvironment in acute ischemic stroke. *Adv Sci*. 2021;8:e2101526. doi:10.1002/advs.202101526

57. Rabiee N, Ahmadi S, Iravani S, et al. Functionalized silver and gold nanomaterials with diagnostic and therapeutic applications. *Pharmaceutics*. 2022;14. doi:10.3390/pharmaceutics14102182

58. Zheng M, Kanneganti TD. The regulation of the ZBP1-NLRP3 inflammasome and its implications in pyroptosis, apoptosis, and necroptosis (PANoptosis). *Immunol Rev*. 2020;297:26–38. doi:10.1111/imr.12909

59. Samir P, Malireddi RKS, Kanneganti TD. The PANoptosome: a deadly protein complex driving pyroptosis, apoptosis, and necroptosis (PANoptosis). *Front Cell Infect Microbiol*. 2020;10:238. doi:10.3389/fcimb.2020.00238

60. Sharma DK, Pattnaik G, Behera A. Recent developments in nanoparticles for the treatment of diabetes. *J Drug Target*. 2023;1–12. doi:10.1080/1061186x.2023.2261077

61. Zhang J, Wang X, Vikash V, et al. ROS and ROS-mediated cellular signaling. *Oxid Med Cell Longev*. 2016;2016:4350965. doi:10.1155/2016/4350965

62. Wu Y, Yao YM, Lu ZQ. Mitochondrial quality control mechanisms as potential therapeutic targets in sepsis-induced multiple organ failure. *J Mol Med*. 2019;97:451–462. doi:10.1007/s00109-019-01756-2

63. Van Heeke G, Allosery K, De Brabandere V, et al. Nanobodies® as inhaled biotherapeutics for lung diseases. *Pharmacol Ther*. 2017;169:47–56. doi:10.1016/j.pharmthera.2016.06.012

64. Eisen DP. Manifold beneficial effects of acetyl salicylic acid and nonsteroidal anti-inflammatory drugs on sepsis. *Intensive Care Med*. 2012;38(8):1249–1257. doi:10.1007/s00134-012-2570-8

65. Fowler AA, Truwit JD, Hite RD, et al. Effect of vitamin C infusion on organ failure and biomarkers of inflammation and vascular injury in patients with sepsis and severe acute respiratory failure: the CITRIS-ALI randomized clinical trial. *JAMA*. 2019;322(13):1261–1270. doi:10.1001/jama.2019.11825

66. Liu D, Huang SY, Sun JH, et al. Sepsis-induced immunosuppression: mechanisms, diagnosis and current treatment options. *Military Med Res*. 2022;9(1):56. doi:10.1186/s40779-022-00422-y

67. Fowler AA. Vitamin C: rationale for its use in sepsis-induced acute respiratory distress syndrome (ARDS). *Antioxidants*. 2024;13(1):95.